2014

ARF and p53 coordinate tumor suppression of an oncogenic IFN-β-STAT1-ISG15 signaling axis

Jason T. Forys
Washington University School of Medicine in St. Louis

Catherine E. Kuzmicki
Washington University School of Medicine in St. Louis

Anthony J. Saporita
Washington University School of Medicine in St. Louis

Crystal L. Winkeler
Washington University School of Medicine in St. Louis

Leonard B. Maggi Jr.
Washington University School of Medicine in St. Louis

See next page for additional authors

OPEN ACCESS
CellPress

Cell Reports
Article

ARF and p53 Coordinate Tumor Suppression of an Oncogenic IFN-β-STAT1-ISG15 Signaling Axis

Jason T. Forys,[1,2] Catherine E. Kuzmicki,[1,2] Anthony J. Saporita,[1,2] Crystal L. Winkeler,[1,2] Leonard B. Maggi, Jr.,[1,2] and Jason D. Weber[1,2,3,*]
[1]BRIGHT Institute
[2]Division of Molecular Oncology, Department of Internal Medicine
[3]Department of Cell Biology and Physiology
Siteman Cancer Center, Washington University School of Medicine, Saint Louis, MO 63110, USA
*Correspondence: jweber@dom.wustl.edu
http://dx.doi.org/10.1016/j.celrep.2014.03.026

SUMMARY

The ARF and p53 tumor suppressors are thought to act in a linear pathway to prevent cellular transformation in response to various oncogenic signals. Here, we show that loss of p53 leads to an increase in ARF protein levels, which function to limit the proliferation and tumorigenicity of *p53*-deficient cells by inhibiting an IFN-β-STAT1-ISG15 signaling axis. Human triple-negative breast cancer (TNBC) tumor samples with coinactivation of p53 and ARF exhibit high expression of both STAT1 and ISG15, and TNBC cell lines are sensitive to STAT1 depletion. We propose that loss of p53 function and subsequent ARF induction creates a selective pressure to inactivate ARF and propose that tumors harboring coinactivation of ARF and p53 would benefit from therapies targeted against STAT1 and ISG15 activation.

INTRODUCTION

The *CDKN2A* and *TP53* tumor-suppressor genes are two of the most frequently inactivated genomic loci in human cancers (Sherr et al., 2005). *CDKN2A* encodes two unrelated proteins, $p14^{ARF}$ ($p19^{ARF}$ in mice) and $p16^{INK4A}$, both of which function as tumor suppressors (Quelle et al., 1995). This unprecedented genomic organization leads to the sharing of exons 2 and 3 by ARF and p16, but due to distinct promoters and first exons, ARF is translated in an alternative reading frame, hence its name. p16 is a well-characterized cyclin-dependent kinase inhibitor, and functions to keep the retinoblastoma protein (Rb) in a hypophosphorylated state, effectively blocking entry into S phase of the cell cycle (Roussel, 1999). ARF, in response to hyperproliferative and hypergrowth cues, induces p53 stabilization by binding to and sequestering the p53 E3 ubiquitin ligase MDM2 in the nucleolus (Saporita et al., 2007; Zindy et al., 1997). Relief of the inhibitory effects of MDM2 allows p53 to activate transcriptional programs leading to cell-cycle arrest or apoptosis (Riley et al., 2008). Thus, ARF and p53 are thought to function in a linear genetic pathway that functions to protect cells from inappropriate oncogenic signaling (Sherr, 2001).

Since ARF's initial discovery, it has been observed that cells lacking p53 function contain elevated levels of ARF (Quelle et al., 1995; Stott et al., 1998; Zindy et al., 1998). A mechanistic explanation for this phenomenon surfaced when it was recently shown that p53 is a potent transcriptional repressor of the *CDKN2A* promoter. Recruitment of histone deacetylases and Polycomb group proteins by p53 renders the locus inaccessible to transcription factors (Zeng et al., 2011). Thus, in the context of p53 loss of function, ARF transcription is derepressed and protein levels become elevated. It is heavily debated whether these induced protein levels are functional.

Mounting evidence suggests ARF possesses important p53-independent tumor-suppressor functions, supported by the findings that *TP53* and *CDKN2A* are frequently coinactivated in human cancers (Cancer Genome Atlas Research Network, 2012; O'Dell et al., 2012; Rozenblum et al., 1997; Sanchez-Cespedes et al., 1999; Saporita et al., 2007; Sherr, 2006). Admittedly, it remains unclear which *CDKN2A* gene product, ARF or p16, is selected against in tumors. However, several groups have shown that *p53*-null cells are sensitive to exogenous overexpression of ARF, demonstrating that ARF can function independently of p53 to inhibit proliferation and suggesting a selective pressure might exist to selectively silence ARF in the absence of *p53* (Sherr, 2006; Sherr et al., 2005; Weber et al., 2000). Here, we show that acute p53 loss results in an induction of ARF protein expression and that this endogenous ARF accumulation functions to limit the proliferation and tumorigenicity of *p53*-deficient cells. Furthermore, we demonstrate that this elevated ARF expression inhibits a protumorigenic signaling cascade mediated by interferon β (IFN-β) secretion and activation of the STAT1 transcription factor. We propose that in the absence of both p53 and ARF, IFN signaling is undeterred and cellular transformation is enhanced, a finding that we substantiate in primary human breast cancers.

RESULTS

Acute p53 Loss Induces Functional ARF

It has long been assumed that the high levels of ARF found in *p53*-deficient cells are not tumor suppressive. To directly

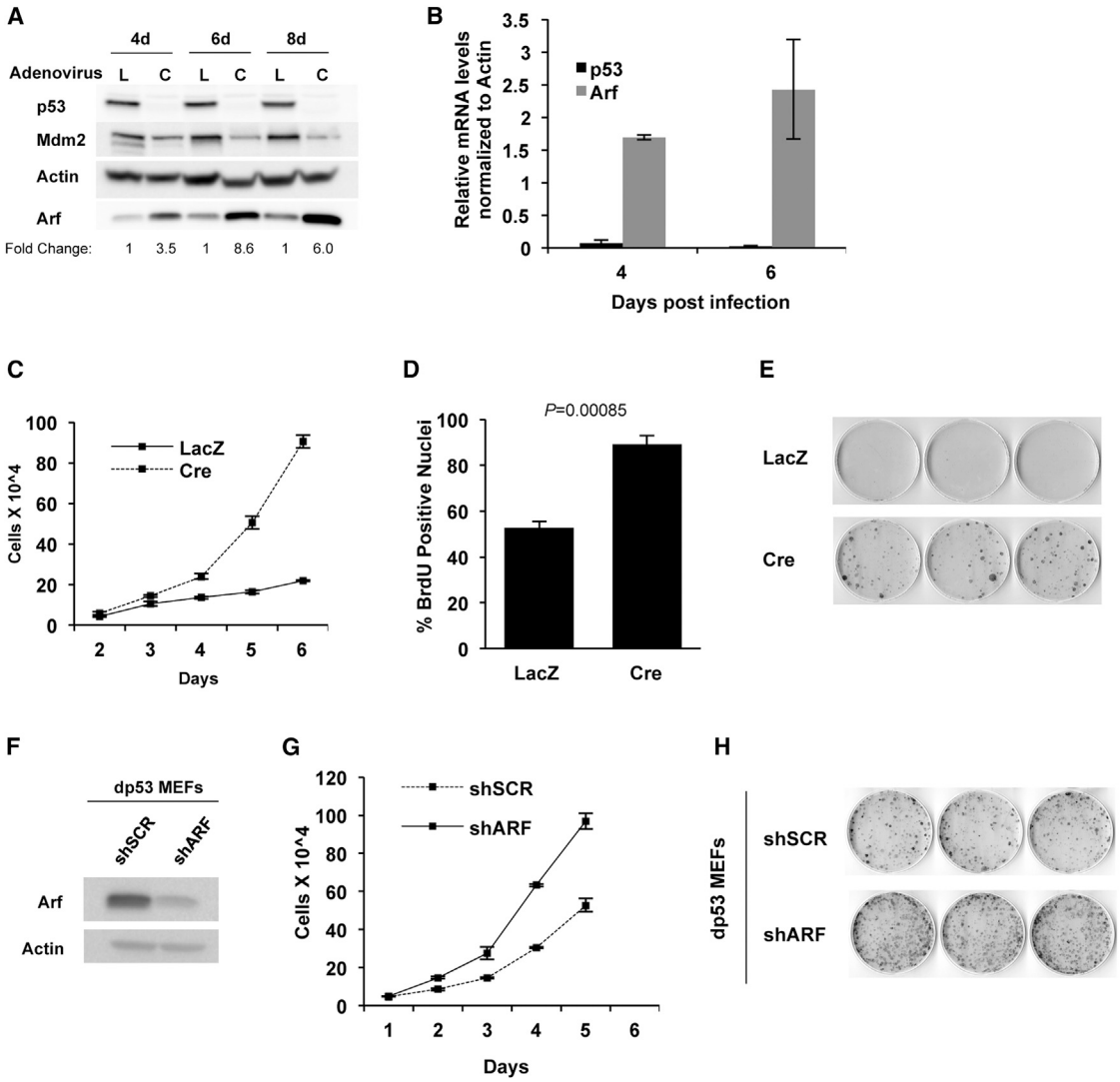

Figure 1. Acute Loss of p53 Induces Functional ARF

(A) Western blot analysis of cell lysates from *p53*$^{flox/flox}$ MEFs infected with Ad-LacZ (L) or Ad-Cre (C) harvested at the indicated time points. Fold change of ARF levels are relative to Ad-LacZ control.

(B) qRT-PCR analysis of p53 and ARF mRNA levels from *p53*$^{flox/flox}$ MEFs infected with Ad-LacZ or Ad-Cre. mRNA levels were normalized to β-actin, and fold changes are relative to Ad-LacZ controls. Error bars represent SD for n = 3 from three independent experiments.

(C) Proliferation assay performed with cells described in (A) and (B).

(D) Ad-LacZ- or Ad-Cre-infected *p53*$^{flox/flox}$ MEFs pulsed with BrdU for 4 hr. BrdU- and DAPI-positive nuclei were visualized using immunofluorescence, and data represent percent BrdU-positive nuclei from three independent experiments.

(E) Representative image of foci assay with Ad-LacZ or Ad-Cre infected *p53*$^{flox/flox}$ MEFs.

(F) Western blot analysis of dp53 MEFs infected with shSCR or shARF.

(G) Equal numbers of dp53 MEFs infected with shSCR or shARF were plated and manually counted on the indicated days.

(H) Representative image of foci assay performed with dp53 MEFs expressing shSCR or shARF.

See also Figure S2.

address this assumption, we utilized a conditional mouse model of p53 inactivation where exons 2–10 are flanked by *loxP* sites (Jonkers et al., 2001). Adenoviral (Ad) delivery of Cre-recombinase into *p53*$^{flox/flox}$ mouse embryonic fibroblasts (MEFs) resulted in an accumulation of ARF mRNA and protein by 4 days postinfection, and levels continued to rise over time and passage (Figures 1A and 1B). These data are in agreement with previous findings that p53 directly binds to and is capable of repressing the ARF promoter (Zeng et al., 2011). Importantly, a transcriptional target of p53, MDM2, was reduced following excision of *p53* (Figure 1A).

These *p53*$^{\Delta/\Delta}$ MEFs, hereafter referred to as dp53 cells (deleted for p53), proliferated faster than LacZ-infected controls, exhibited more rapid S phase entry, and formed numerous foci

when plated at low density (Figures 1C–1E). Infection of dp53 MEFs with a short hairpin RNA (shRNA) specifically targeting ARF resulted in further enhancement of proliferation and foci formation (Figures 1F–1H), indicating that the proliferation of *p53*-deficient cells is constrained by endogenously induced ARF protein. Importantly, shRNA-mediated depletion of ARF did not reduce p16 levels, indicating the observed enhancement of proliferation was specifically due to ARF loss (Figure S2A).

Endogenous ARF Limits the Tumorigenicity of *p53*-Deficient Cells

To test the tumor-suppressive functions of ARF in the context of *p53* loss, we overexpressed mutant H-Ras^{V12} in dp53 MEFs and then depleted ARF (Figure 2A). As seen in Figure 2, Ras^{V12}-transformed dp53 MEFs (dp53R MEFs) were capable of forming colonies in soft agar (Figure 2B, top left panel). However, depletion of ARF in the dp53R MEFs resulted in a tremendous increase in the size of soft agar colonies, indicating an increase in tumorigenic potential (Figures 2B and 2C). The dp53R-shARF MEFs also exhibited higher proliferative rates, bromodeoxyuridine (BrdU) incorporation rates, and increased foci formation compared to dp53R-shSCR cells, supporting our observed tumorigenic phenotype (Figures 2D–2F). To extend our findings in vivo, we injected the dp53R-shARF cells into the flanks of nude mice. We observed a striking enhancement in the growth kinetics of dp53R-shARF tumors relative to tumors formed with dp53R-shSCR cells (Figures 2G and 2H). Taken together, these data demonstrate the endogenous ARF levels that accumulate following *p53* loss function to limit tumorigenicity.

ARF Inhibits an Interferon-Sensitive Gene Signature Induced upon *p53* Loss

Having demonstrated that the induced levels of ARF in *p53*-deficient cells serve a tumor-suppressive function (Figure 2), we sought to understand which oncogenic processes ARF might be inhibiting to limit tumorigenicity. The previously ascribed p53-independent tumor-suppressive roles of ARF include regulating general or mRNA-specific translation (Apicelli et al., 2008; Kawagishi et al., 2010; Kuchenreuther and Weber, 2014; Sugimoto et al., 2003), inhibition of transcription factors such as c-Myc (Qi et al., 2004), and modulation of protein sumoylation (Kuo et al., 2008). We analyzed these processes in our system and observed no significant differences between dp53R-shSCR and dp53R-shARF MEFs (data not shown).

Therefore, we took an unbiased approach to identify changes in global mRNA expression between dp53R-shSCR and dp53R-shARF MEFs. Comparative microarray analysis yielded numerous upregulated immune response genes in the dp53R-shARF cells, including *Irf7*, *Oasl2*, *Ifit3*, *Usp18*, *Mx2*, and *Isg15* (Figures 3A and 3B). Pathway analysis indicated that the gene signature was most strongly associated with the innate immune response or type I IFN response (Figure 3B). The interferon-sensitive gene (ISG) expression changes were validated by quantitative RT-PCR (qRT-PCR) (Figure 3C).

As an important control, we analyzed ISG expression in our cell lines following infection with the various viral constructs used in our experiments and compared to mRNA levels in "mock"-infected cells (no virus). Retroviral infection with empty vector or Ras^{V12} did not induce ISGs, and lentiviral infection of *Arf*-null or wild-type MEFs with shSCR or shARF had no effect on ISG mRNA levels (Figures S1A–S1C). Furthermore, a comparison of three different low-passage (<passage 6) wild-type and *Arf*-null MEF lines showed no increase in ISG expression (Figure S1D). The only genetic setting where ARF depletion induced ISGs was in the context of *p53* deficiency (Figure S1E). Additional experiments were performed to assess the role of p16INK4a in ISG induction. As shown in Figure S2, an shRNA targeting both ARF and p16 was unable to induce an additive effect on ISG expression (Figures S2B and S2C). Moreover, specific depletion of p16 in dp53R MEFs did not induce ISG expression (Figures S2D and S2E). Thus, ARF's inhibition of ISG expression is entirely dependent on a *p53*-deficient genetic setting, and p16 knockdown does not produce the same effects.

Given ARF's ability to inhibit ISG expression exclusively in the context of *p53* deficiency, we hypothesized that loss of *p53* might be the driving force behind upregulation of the ISGs and that the induction of ARF would then serve as a biological "brake" to suppress the response. To test this hypothesis, we analyzed ISG mRNA expression following infection of *p53*$^{flox/flox}$ MEFs with Ad-Cre or -LacZ control. As shown in Figure 3D, expression of ISG15 and OASL2 are induced at 4 and 6 days after *p53* loss. Consistent with our hypothesis, 8 days after *p53* loss, when ARF protein levels are maximally induced, we no longer observed a significant induction of the ISGs (Figures 3D and 3E). The suppression of ISG15 and OASL2 expression 8 days after *p53* loss was completely relieved when ARF-specific shRNA was introduced. Therefore, the negative feedback p53 imposes on ARF exists to allow ARF to respond to acute *p53* loss by inhibiting an induction of ISGs.

Having demonstrated ARF and p53 cooperate to suppress expression of ISGs in vitro, we sought to establish the existence of this signaling pathway in vivo. We generated cohorts of *Blg-Cre;p53*$^{flox/flox}$*;Arf*$^{+/+}$ and *Blg-Cre;p53*$^{flox/flox}$*;Arf* $^{flox/flox}$ mice to analyze the effects of losing *p53* alone versus losing both *Arf* and *p53*. Activation of Cre-recombinase by the beta-lactoglobulin (Blg) promoter induces recombination of floxed alleles specifically in the mammary gland of lactating female mice (Selbert et al., 1998). Tumors isolated from *Blg-Cre;p53*$^{flox/flox}$*;Arf* $^{flox/flox}$ mice expressed 3.5-fold more ISG15 mRNA than those obtained from *Blg-Cre;p53*$^{flox/flox}$*;Arf* $^{+/+}$ mice (Figures S3A and S3B). This result is in support of the hypothesis that p53 and ARF cooperate to suppress ISG expression in vivo and clearly demonstrates the observed ISG induction is not simply an artifact of tissue culture.

IFN-β Is Necessary and Sufficient for Increased Tumorigenicity in dp53R-shARF MEFs

Our microarray data and pathway analysis indicated an activation of the type I IFN response, or more specifically, response to IFN-β. We analyzed IFN-β mRNA expression using qRT-PCR in our dp53R-shARF MEFs and consistently observed a 2- to 3-fold induction (Figure 4A). Additionally, this 3-fold induction of IFN-β mRNA resulted in a nearly 11-fold increase in IFN-β secretion in the media containing dp53R-shARF cells as measured by ELISA (Figure 4B). To determine the requirement of secreted IFN-β for cell proliferation, we knocked down IFN-β in dp53R-shARF cells. This resulted in a significant decrease in

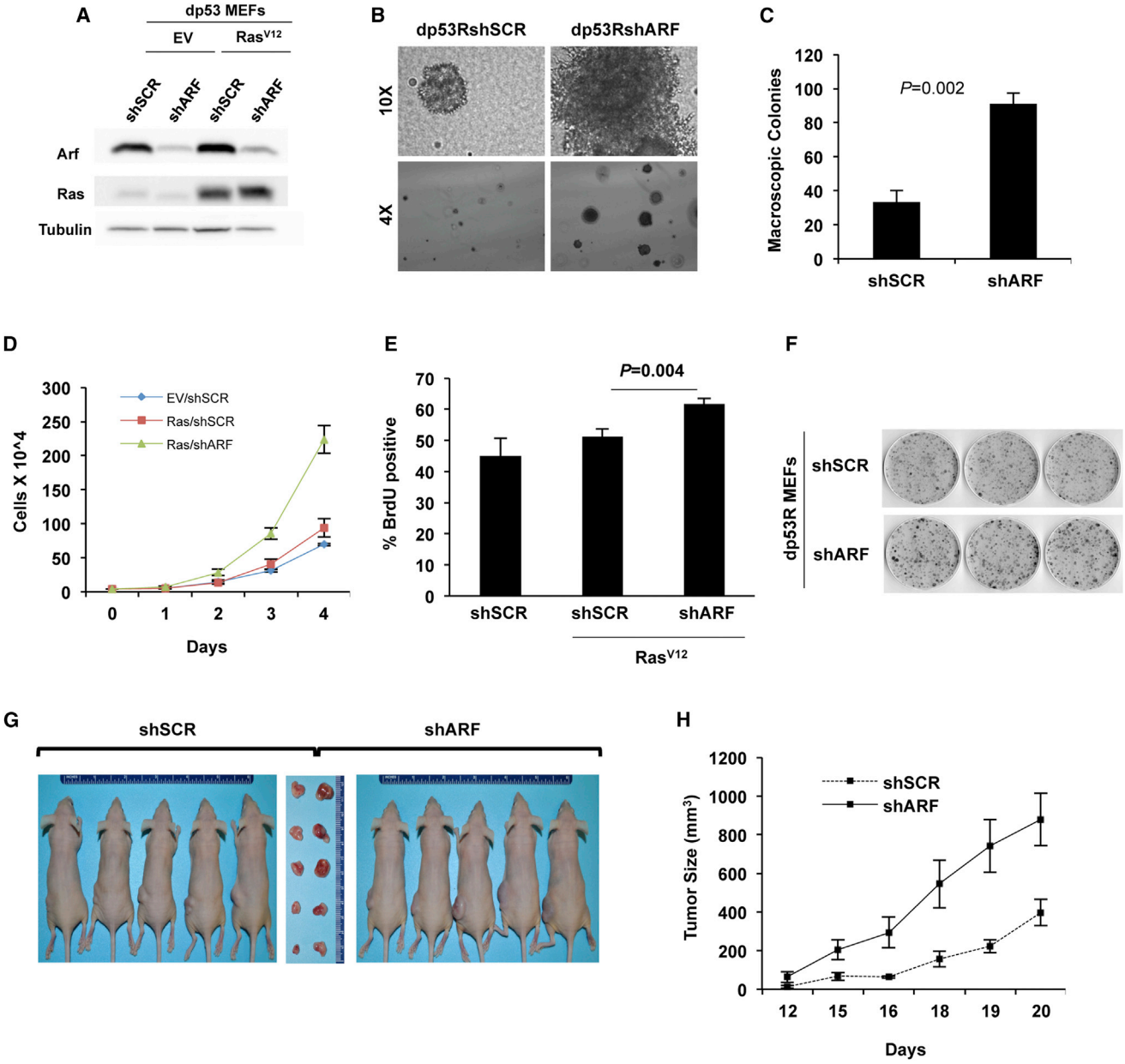

Figure 2. Endogenous ARF Limits the Tumorigenicity of p53-Deficient Cells

(A) Western blot analysis of dp53 MEFs expressing Ras^{V12} (dp53R) and infected with shSCR or shARF.

(B and C) Representative images of dp53R-shSCR or dp53R-shARF MEFs growing in soft agar. Macroscopic colonies were quantified in (C). Error bars represent SD of n = 3.

(D) Proliferation assay of dp53 MEFs expressing empty vector or Ras^{V12} and infected with shARF or shSCR control.

(E) Percent BrdU-positive nuclei of cells described in (D) following 4 hr pulse with BrdU. Error bars represent SD from three independent measurements of 100 nuclei.

(F) Representative image of foci assay performed with dp53R MEFs expressing shSCR or shARF.

(G) Images of tumor-bearing mice and excised tumors from allograft experiments using dp53R-shARF or shSCR MEFs.

(H) Tumor size was measured using calipers on the indicated days postinjection. Tumor size (volume) was calculated as described in Experimental Procedures. Error bars represent SD of n = 5.

both IFN-β expression and phosphorylated STAT1 (Figures 4C and 4D). Long-term proliferation was significantly impaired in cells with reduced IFN-β (Figure 4E), indicating a requirement for IFN-β production in dp53R-shARF cells.

Next, we sought to determine if enhanced production of IFN-β was sufficient to promote the aberrant proliferation of dp53R cells in the presence of high ARF levels. Using concentrations of recombinant IFN-β that matched the concentration range

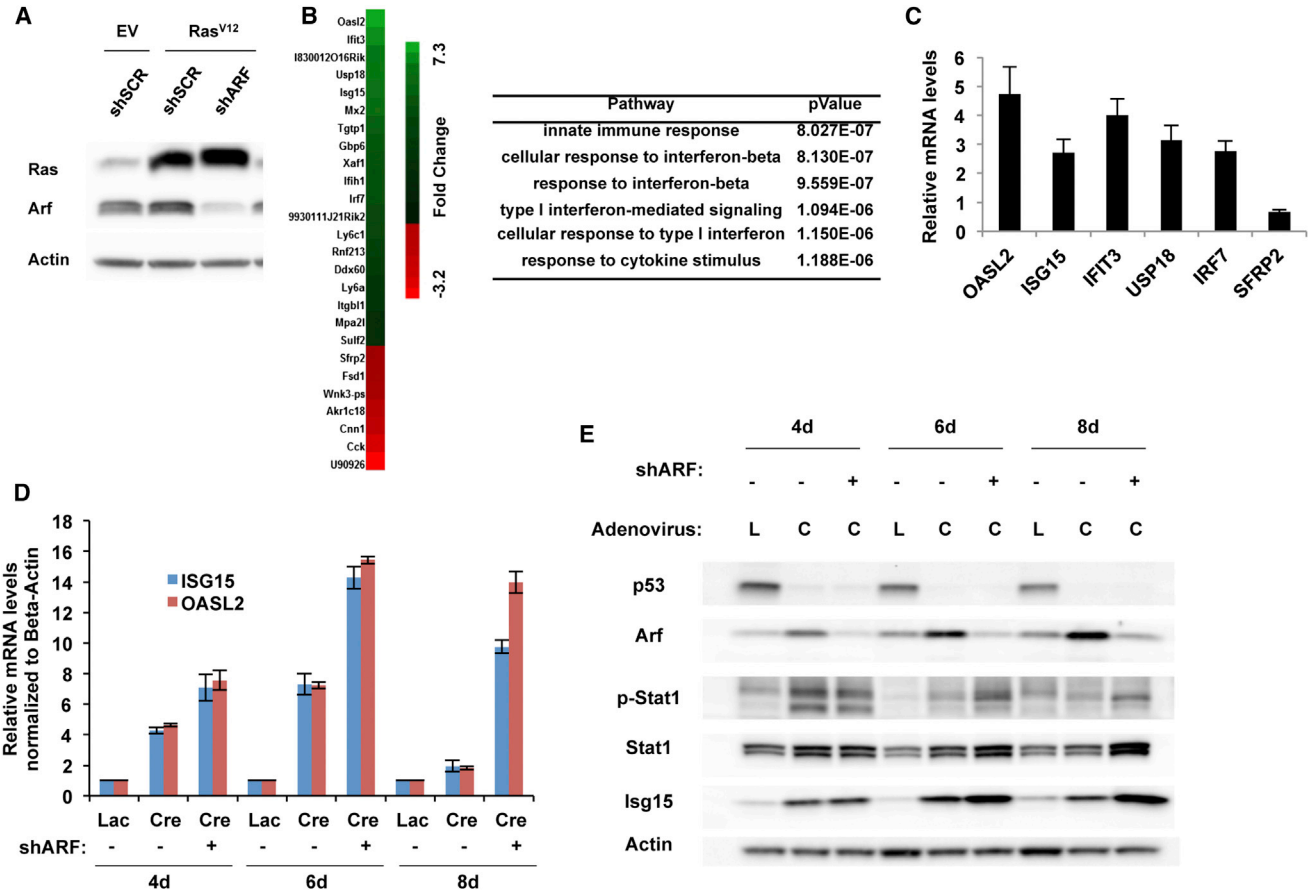

Figure 3. ARF Inhibits an Interferon-Sensitive Gene Signature Induced upon *p53* Loss

(A) Western blot verifying overexpression of Ras^{V12} and knockdown of ARF in dp53 MEFs. RNA from three independent experiments was submitted for microarray analysis.

(B) Heatmap showing significantly altered genes (>2-fold change) and pathway analysis of significantly altered genes in the data set.

(C) Validation of ISGs with qRT-PCR. Levels were normalized to histone 3.3 mRNA and are relative to shSCR controls. Error bars represent SD from three independent experiments.

(D) qRT-PCR analysis of $p53^{flox/flox}$ MEFs infected with Ad-LacZ or Ad-Cre from the indicated time points postinfection. Cells were all infected with shSCR(−) or shARF(+) 1 day after Cre-infection as indicated. mRNA levels are relative to Ad-LacZ-shSCR controls and represent averages of three independent experiments.

(E) Western blot analysis of cells described in (D).

See also Figures S1–S3.

detected in the media of dp53R-shARF cells, we observed a significant increase in long-term proliferation of dp53R cells that was comparable to that seen in dp53R-shARF cells (Figure 4G). Markedly, recombinant IFN-β stimulated ISG15 expression to the same level seen in dp53R-shARF cells (Figure 4F). Therefore IFN-β production is sufficient to phenocopy the signaling pathway activation and proliferative gains seen with ARF knockdown in dp53R cells.

ARF Represses a Protumorigenic STAT1-ISG15 Signaling Cascade

Canonical IFN-β signaling occurs upon ligand binding to the membrane receptors IFNAR1/2. Upon ligand binding, a conformational change allows autophosphorylation of receptor-bound JAK1 and TYK2. The activation of these kinases leads to phosphorylation of STAT1 and STAT2 proteins, which enables them to enter the nucleus. Once inside the nucleus, the STAT1/STAT2 heterodimer associates with IRF9 to form a complex known as interferon-stimulated gene factor 3 (ISGF3), which is fully capable of initiating transcription of genes containing interferon-stimulated response elements (ISREs) (Platanias, 2005). Many of the genes in our ISG signature contain ISREs in their promoters (Sadler and Williams, 2008), and it is well established that activation of the STAT1 transcription factor is required for upregulation of ISRE-containing genes (Ramana et al., 2000). Therefore, we analyzed STAT1 status in dp53R-shARF cells and observed increases in the phosphorylation of both tyrosine 701 and serine 727 activation sites as well as an accumulation of total STAT1 levels (Figure 5A). Neither STAT3 activation nor increased expression of its upstream cytokine, interleukin-6, was observed in the same genetic context (Figure S4). The increase in total STAT1 was due to an increase in mRNA levels,

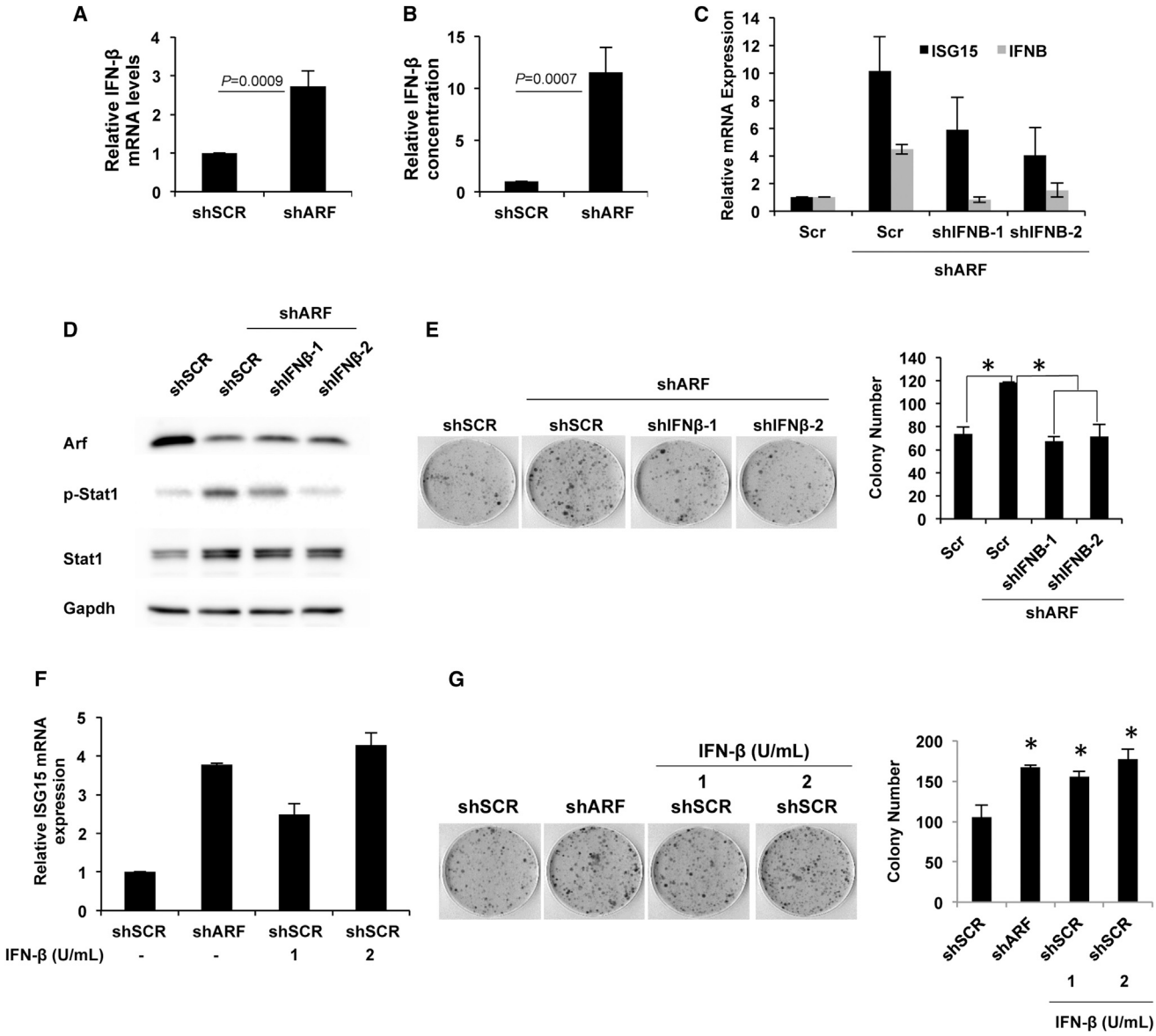

Figure 4. IFN-β Signaling Is Necessary and Sufficient for Enhanced Tumorigenicity in dp53R-shARF MEFs

(A) qRT-PCR analysis of IFN-β mRNA levels in dp53R-shARF MEFs. Levels are normalized to histone 3.3 mRNA and relative to shSCR controls.

(B) Extracellular IFN-β concentration measured by ELISA in dp53R-shARF MEFs. Values are fold changes relative to shSCR control. Error bars represent SD of three independent experiments.

(C) qRT-PCR analysis of dp53R-shSCR or -shARF MEFs infected with two specific shRNAs targeting IFN-β. Relative mRNA expression was obtained by normalizing to histone 3.3 mRNA. Error bars represent SD of three independent measurements.

(D) Western blot analysis of cells described in (C) for the indicated proteins.

(E) Representative image of foci assay performed with dp53R-shARF or shSCR MEFs infected with two IFN-β-specific shRNAs. Quantification of three independent measurements is shown (right).

(F) qRT-PCR analysis of dp53R-shSCR or –shARF cells treated with the indicated concentration of IFN-β. Error bars represent SD of values from three independent measurements.

(G) Representative image of foci assay performed with dp53R-shARF or shSCR MEFs treated with the indicated concentration of recombinant IFN-β. Quantification of three independent measurements is shown (right). *p < 0.01

consistent with the observation that the STAT1 promoter contains an ISRE (Figure 5B) (Zimmerman et al., 2012).

To test whether STAT1-mediated signaling was required for the increased tumorigenicity in the dp53R-shARF MEFs, we used shRNAs to deplete STAT1. Reducing total STAT1 protein levels led to a concomitant decrease in phosphorylation in dp53R-shARF MEFs (Figure 5C). As shown in Figure 5D, mRNA expression of select ISGs was also reduced following

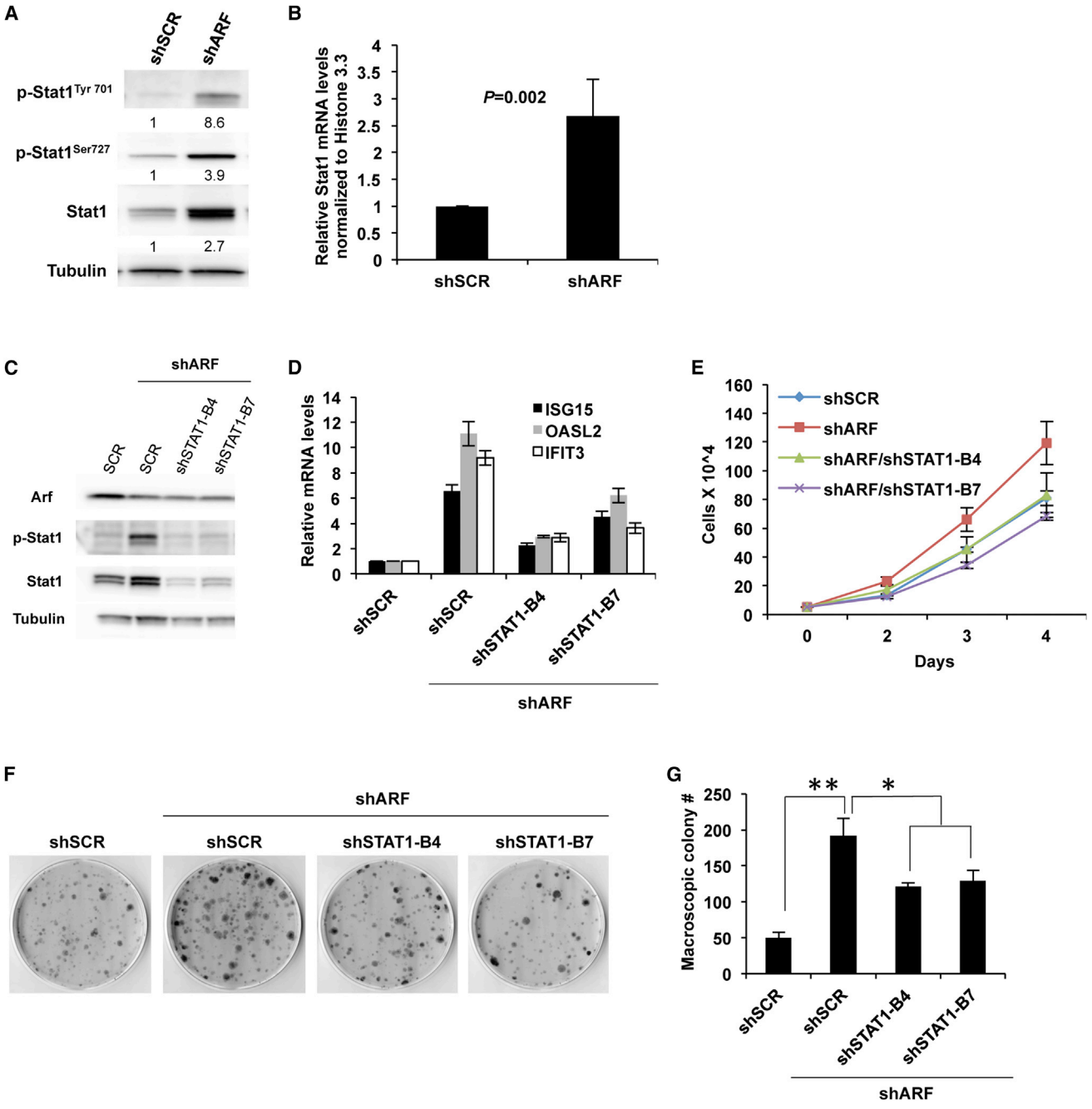

Figure 5. STAT1 Activation Is Required for Increased Tumorigenicity in dp53R-shARF MEFs

(A) Western blot analysis of dp53R-shARF or shSCR MEFs showing STAT1 activation.

(B) qRT-PCR analysis of total STAT1 mRNA levels in dp53R-shARF MEFs. mRNA levels are relative to shSCR controls and normalized to histone 3.3.

(C) Western blot analysis of dp53R-shSCR or shARF MEFs infected with two different STAT1 shRNAs.

(D) qRT-PCR analysis of dp53R-shSCR or shARF MEFs infected with control or two different STAT1 shRNAs.

(E) Proliferation assay of dp53R MEFs expressing the indicated shRNAs.

(F) Representative images of foci assays with dp53R MEFs expressing the indicated shRNAs.

(G) Soft agar quantification of STAT1-depleted dp53R-shARF MEFs.

All error bars represent SD for n = 3. *p < 0.0004, **p < 0.009. See also Figure S4.

STAT1 knockdown. Short and long-term proliferation of dp53R-shARF MEFs was inhibited and colony growth in soft agar was reduced (Figures 5E–5G). Taken together, these data indicate that ARF protects *p53*-deficient cells from inappropriate STAT1 activation and, if left unchecked, signaling through STAT1 can lead to increased tumorigenicity.

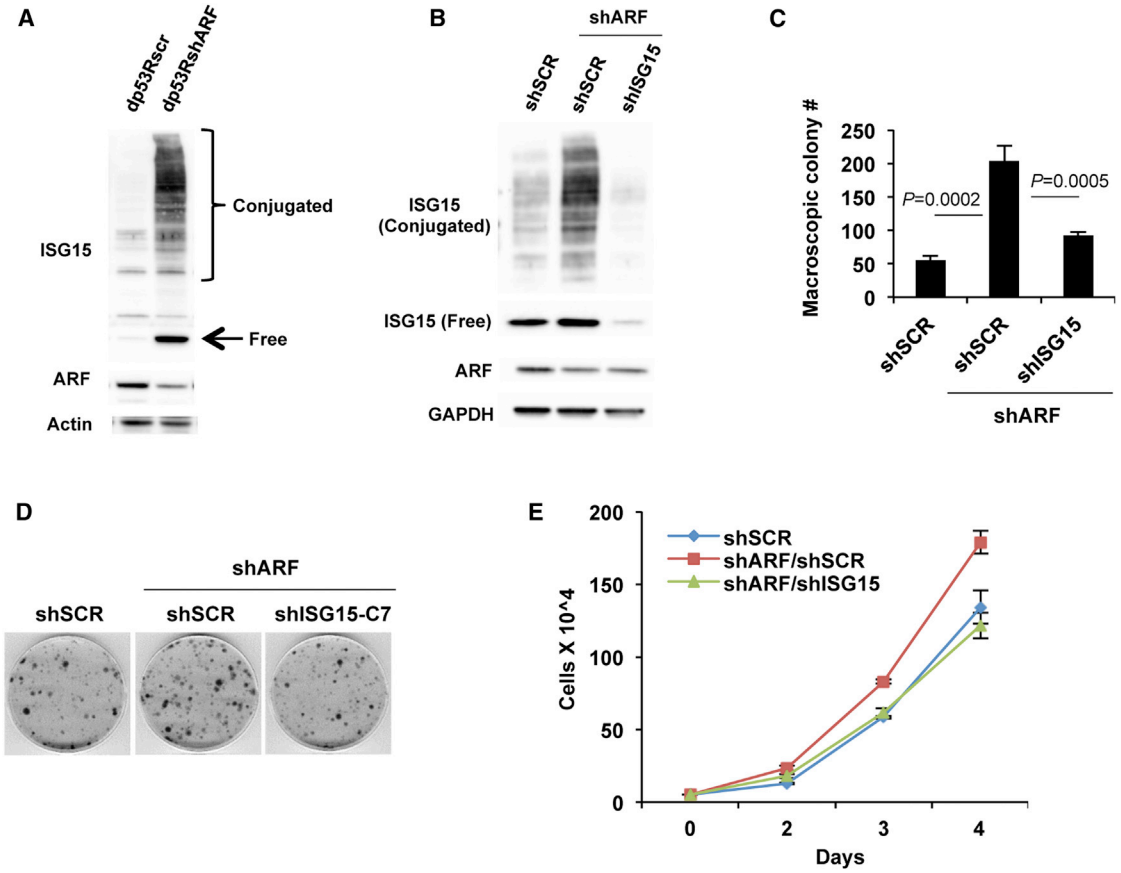

Figure 6. ISG15 Is Required for Increased Tumorigenicity in dp53R-shARF MEFs

(A) Western blot analysis of ISG15 expression in dp53R-shARF MEFs. Free and conjugated forms are indicated.

(B) Western blot analysis of dp53R-shSCR or shARF MEFs expressing an shRNA specifically targeting ISG15.

(C) Quantification of macroscopic soft agar colony number with cells described in (B).

(D) Representative image of foci experiment from dp53R MEFs infected with the indicated shRNAs.

(E) Proliferation assay for dp53R MEFs infected with the indicated shRNAs.

All error bars represent SD of n = 3.

Interestingly, one of the IFN-responsive genes, *Isg15*, encodes a ubiquitin-like protein that is conjugated to lysine residues and has recently been shown to be required for the tumorigenicity of select breast cancer cell lines (Burks et al., 2014). Increased ISG15 expression in dp53R-shARF MEFs is dependent upon STAT1 (Figure 5D), so we hypothesized ISG15 might represent one of the protumorigenic targets activated downstream of STAT1. Western blot analysis confirmed upregulation of both free and conjugated species of ISG15 in dp53R-shARF cells (Figure 6A). Using an shRNA specific to ISG15, we observed a significant reduction in soft agar growth, foci formation, and proliferation in the dp53R-shARF MEFs upon ISG15 knockdown (Figures 6B–6E), indicating that elevated ISG15 is required for the tumorigenesis of dp53R-shARF cells.

Analysis of TNBC Patient Samples and Cell Lines

We have demonstrated that ARF protein induced by *p53* loss protects against the tumorigenic accumulation of an ISG signature in a mouse model system. To investigate whether this pattern of regulation was conserved in human cells, we focused on triple-negative breast cancer (TNBC) because over 80% of these patients harbor p53 mutations (Ellis and Perou, 2013). We performed immunohistochemical analysis on an annotated breast cancer tissue array and scored the triple-negative cores (Table S1). Whereas elevated expression of ARF would be expected in the presence of p53 mutation, we observed that 11 of the 13 samples with p53 mutation exhibited low or no ARF staining, suggesting coinactivation of both ARF and p53. Further, 6 of 11 tissues with both ARF and p53 loss of function displayed intense staining of STAT1 and ISG15 (Figures 7A and 7B).

Finally, we analyzed a panel of five TNBC cell lines. The HCC70 cell line, which displayed high ARF protein expression, was resistant to STAT1 depletion (Figures 7C, 7D, and S5A). The other four cell lines, which did not express ARF, were all extremely sensitive to STAT1 depletion, displaying signs of cytotoxicity (Figures 7C, 7D, and S5B). The short hairpins targeting STAT1 did not reduce STAT3, a known promoter of breast

A

TNBC IHC Statistics

p53^{mutant}	✚	High ARF		2/13 (15%)
p53^{mutant}	✚	Low/No ARF		11/13 (85%)
p53^{mutant}	✚	Low/No ARF	✚ High STAT1/ISG15	6/11 (55%)

B

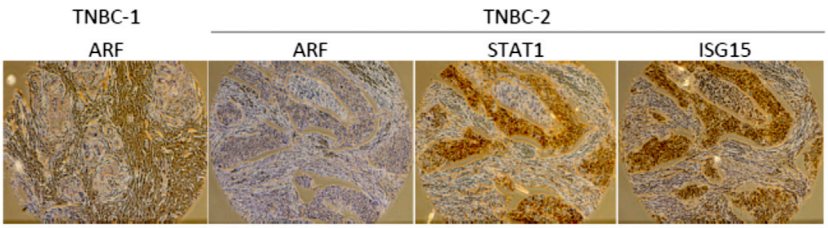

C

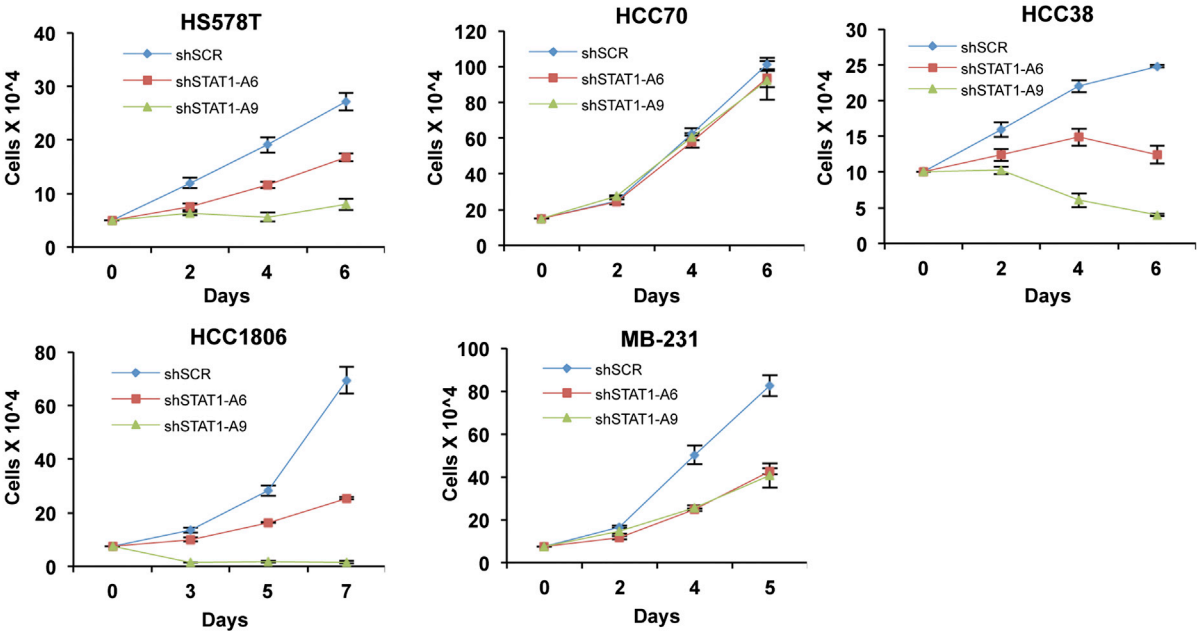

D

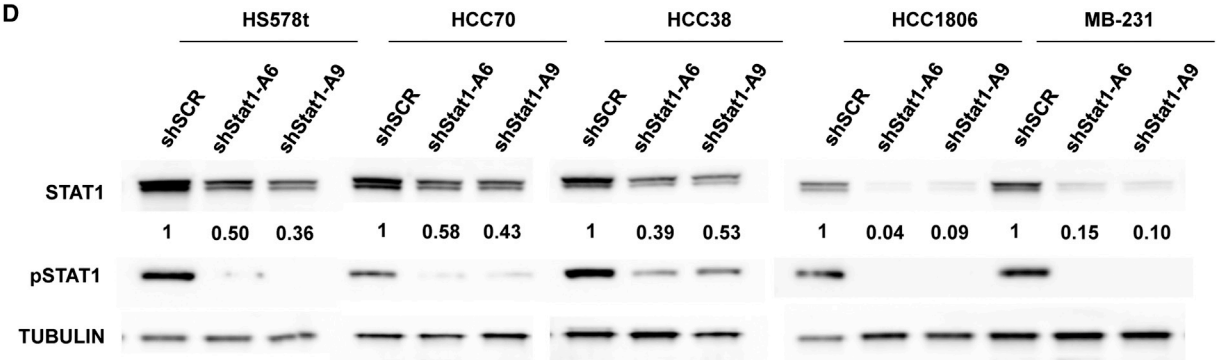

(legend on next page)

cancer tumorigenesis (Marotta et al., 2011) (Figure S5C), confirming the selective requirement of STAT1 activation in controlling the proliferation of these cells. Interestingly, the HCC70 cell line that was resistant to STAT1 depletion also expressed the highest level of ISG15 among the TNBC cell lines assayed (Figure S5A). We hypothesized that this cell line might have upregulated ISG15 independently of STAT1-mediated transcription. In agreement with this hypothesis, depletion of STAT1 in HCC70 cells did not reduce ISG15 levels (Figure S6A). Given our results in Figure 6, which indicated ISG15 is one of the key protumorigenic effectors upon ARF depletion, we tested whether depleting ISG15 in HCC70 cells would inhibit their proliferation. Indeed, shRNA-mediated reduction of ISG15 significantly reduced HCC70 cell proliferation (Figures S6B and S6C). Taken together, these data demonstrate that inhibition of type I IFN signaling components like STAT1 and ISG15 can inhibit proliferation of TNBC cell lines and also that other deregulated pathways in addition to ARF/p53 are likely capable of inducing ISG expression.

DISCUSSION

Our work has provided an answer to a long-standing question in cancer biology: What biological advantage does a normal cell gain by having the p53 tumor suppressor repress transcription of another tumor suppressor, ARF? We have shown that loss of *p53* leads to a potent induction of ARF protein levels and that this large endogenous pool of ARF functions to limit proliferation and tumorigenicity in the face of oncogenic transformation.

To our surprise, depletion of ARF in *p53*-deficient cells led to an induction of ISGs through secretion of IFN-β and activation of the transcription factor STAT1. Our data further demonstrated collaboration of p53 and ARF in suppressing STAT1 signaling activation and subsequent ISG transcriptional activation both in vitro and in vivo. This cooperation was specific to p53 and ARF, because p16 was not shown to be important in suppressing ISG expression. Therefore, we propose that loss of p53 leads to two important events: induction of ISGs and the induction of ARF protein levels. Once ARF protein levels reach maximal expression, the transcription of ISGs is inhibited. In these cells, deletion or mutation of the *Arf* locus would predict an upregulation of the IFN gene signature and a subsequent tremendous growth advantage. Therefore, our results suggest a selective pressure does exist to coinactivate both ARF and p53, which indeed occurs in several cancer types (Cancer Genome Atlas Research Network, 2012; O'Dell et al., 2012; Rozenblum et al., 1997; Sanchez-Cespedes et al., 1999).

Mechanistically, we do not yet understand how loss of p53 acts to induce expression of ISGs or how ARF functions to suppress the response. However, several recent publications are in support of our findings and provide potential mechanistic explanations. Cheon et al. showed that loss of p53 can induce unphosphorylated STAT1, which was shown to function in an unphosphorylated ISGF3 (U-ISGF3) complex to induce expression of select ISGs, providing resistance to DNA damaging agents (Cheon et al., 2013). Many of these ISGs overlap with the ones in our gene expression profile. Intriguingly, they also demonstrated that low-level IFN-β, comparable to the levels used in our studies, was capable of inducing activity of this U-ISGF3 complex (Cheon et al., 2013). A recent report has also suggested p53 is involved in suppressing the expression of dsRNA from noncoding portions of the mouse genome (Leonova et al., 2013). An increase in cellular dsRNA as a result of endogenous insults can activate a type I IFN response (Chiappinelli et al., 2012). Future studies will be necessary to explore these possibilities. With regards to suppression of ISG expression by ARF, we have demonstrated that ARF and STAT1 can interact in dp53 MEFs, and we are currently working to understand the biological significance of this interaction (J.T.F., unpublished data).

While the activation of the type I IFN pathway is typically observed in the context of viral defense, numerous groups have found upregulation of this pathway in human cancers (Buess et al., 2007; Duarte et al., 2012; Perou et al., 1999; Zimmerman et al., 2012). The importance of IFN signaling in human cancer is still a debated topic, but most commonly, activation of a type I IFN signature is thought to be tumor suppressive (Chan et al., 2012; Yu et al., 2009). In fact, type I IFN is an approved treatment for many diverse cancer types (Dunn et al., 2006). Our work provides evidence for the direct involvement of IFN-β, STAT1, and a downstream ISG, ISG15, in promoting tumorigenicity. Each of these components was required for the enhanced tumorigenicity we observed in the dp53R-shARF MEFs. Moreover, in cells lacking *p53*, recombinant IFN-β alone was sufficient to stimulate proliferation.

Finally, we identified a subset of TNBC patients harboring coinactivation of ARF and p53 alongside overexpression of STAT1 and ISG15. Additionally, STAT1 depletion in a panel of p53 mutant TNBC cell lines showed that only cells lacking ARF expression were sensitive to the STAT1 shRNAs. Because existing mouse knockout models suggest that normal cells do not require the activity of STAT1 and ISG15 for viability (Durbin et al., 1996; Osiak et al., 2005), targeted therapy of this pathway should be considered ideal for tumor reduction. Moreover, this IFN signaling axis need not be limited to TNBC, because numerous other cancers exhibit concomitant loss-of-function p53 and ARF.

The crosstalk between p53 and ARF has proven to be a multifaceted affair. ARF is induced in response to oncogenic signals

Figure 7. Analysis of TNBC Patient Samples and Cell Lines

(A) Statistics from immunohistochemistry staining of human breast cancer tissue array.

(B) Representative images from immunohistochemistry displaying a section with high ARF staining (TNBC-1) and a section with low/no ARF and high ISG15/STAT1 (TNBC-2).

(C) Proliferation assays of the indicated TNBC cell lines infected with two different STAT1 shRNAs.

(D) Western blot analysis showing STAT1 depletion with shRNAs in various TNBC lines.

See also Figures S5 and S6 and Table S1.

to activate p53; ARF is also induced by loss of p53 to suppress STAT1 signaling. Our findings support a model whereby induction of ARF following p53 loss acts to prevent aberrant IFN-β production and signaling to crucial downstream effectors. Thus, the functional links between p53 and ARF are far more imperative than anticipated. The complex p53-ARF network that we have identified provides tumor-suppressive redundancy where none was thought to exist in cells. We believe our study, combined with several recent reports, indicates a need to more carefully examine the functional importance of IFN signaling in cancer cells to ensure the use of IFN as a treatment option does not produce an undesirable outcome (Burks et al., 2014; Tsai et al., 2011; Zimmerman et al., 2012). Moreover, our work suggests a subset of human cancer patients, those containing p53 and ARF mutations, might benefit from targeted inhibition of STAT1 or ISG15 activation.

EXPERIMENTAL PROCEDURES

Animal Studies

All animal studies were performed according to the guidelines established by the Animal Studies Committee at Washington University in St. Louis. The *p53*$^{flox/flox}$ (FVB.129-*Trp53*^{tm1Brn}) mice were obtained from the National Cancer Institute Mouse Repository and have been previously described (Jonkers et al., 2001).

Cell Culture

Primary MEFs were isolated as previously described (Kamijo et al., 1997). All cells were maintained in Dulbecco's modified Eagle's medium (DMEM) supplemented with 10% fetal bovine serum, 2 mM glutamine, 0.1 mM nonessential amino acids, 1 mM sodium pyruvate, and 2 μg/ml gentamicin. Recombinant IFN-β was obtained from PBL Interferon Source and used at the indicated concentrations.

Viral Production and Infections

Adenoviruses expressing β-galactosidase (Ad-LacZ) or Cre recombinase (Ad-Cre) were purchased from the Gene Transfer Vector Core, University of Iowa. For adenoviral infections, 1 × 10^6 cells were plated in the presence of Ad-LacZ or Ad-Cre (MOI = 50) and incubated for 8 hr. For mutant Ras^{V12} overexpression, retrovirus was produced by transfecting 293T cells with either MSCV-HRAS^{V12}-IRES-GFP plasmid or MSCV-IRES-GFP control and the helper plasmid ψ-2. Virus-containing supernatants were harvested 48 hr posttransfection. Collected retrovirus was used to infect 1 × 10^6 MEFs in the presence of 10 μg/ml polybrene. For the production of lentiviral shRNAs, 293T cells were transfected using Lipofectamine 2000 (Invitrogen) with pCMV-VSV-G, pCMV-ΔR8.2, and pLKO.1-puro constructs. Viral supernatants were harvested 48 hr posttransfection. Cells were infected with lentivirus for 8–12 hr in the presence of 10 μg/ml protamine sulfate. Puromycin was added to cell culture media at a concentration of 2 μg/ml for selection. The sequences of shRNAs are as follows: STAT1-B4 5′-GCCGAGAACATACCAGAGAAT-3′ STAT1-B7 5′- GCT GTTACTTTCCCAGATATT-3′ STAT1-A6 (human) 5′- GAACAGAAATACACCT ACGAA-3′ STAT1-A9 (human) 5′- CTGGAAGATTTACAAGATGAA-3′ ISG15 5′- AGCACAGTGATGCTAGTGGTA-3′ IFN-β-1 5′- GCAGAAGAGTTACACT GCCTT-3′ IFN-β-2 5′- GCAGAGATCTTCAGGAACTTT-3′. The ARF (mouse-specific) hairpin was described previously (Apicelli et al., 2008).

Western Blotting

Cell pellets were lysed and sonicated in EBC lysis buffer (50 mM Tris-Cl [pH 7.4], 120 mM NaCl, 0.5% NP-40, 1 mM EDTA) containing HALT Protease and Phosphatase Inhibitor cocktail (Thermo Scientific) and 1 mM phenylmethanesulfonylfluoride. A total of 30 μg of protein were separated on SDS-polyacrylamide gels. Proteins were transferred to PVDF (Millipore) and probed with antibodies. ARF (mouse), actin, p53 (human), γ-tubulin, H-Ras, ISG15 (human), and STAT1 were all purchased from Santa Cruz Biotechnologies. p53 (mouse), phospho-STAT1^{Tyr701}, phospho-STAT1^{Ser727}, phospho-STAT3^{Tyr705}, and STAT3 were purchased from Cell Signaling. ARF (human) and GAPDH were purchased from Bethyl Laboratories, and MDM2 was from Millipore. The mouse ISG15 antibody was a gift from Dr. Deborah Lenschow. Secondary horseradish peroxidase-conjugated antibodies (Jackson Immunoresearch) were used, and ECL plus was used to visualize the bands (GE Healthcare).

Proliferation, BrdU, and Foci Assays

For proliferation assays, 5–10 × 10^4 cells were plated in six-well plates. Cells were lifted and counted using a hemocytometer at the indicated number of days postplating. For BrdU assays, 1 × 10^4 cells were plated on glass coverslips and incubated overnight. A total of 10 μM BrdU-containing media was added to the cells for 4–6 hr. Cells were fixed with 10% formalin/methanol, and BrdU staining was performed using a BrdU antibody (GE Healthcare) according to the manufacturer's instructions. For foci assays, 3 × 10^3 cells were plated in 10 cm dishes and cells were incubated for 10 days. Cells were fixed with 100% methanol and stained with Giemsa (Sigma Aldrich).

Soft Agar Assay

Cells were lifted and suspended in DMEM containing a final concentration of 0.4% noble agar. A total of 1.5 × 10^4 cells were layered in triplicate onto 0.6% noble-agar/media bottom layer in 60 mm plates. Plates were incubated for 20 days, feeding with media/0.4% agar mix every 6 days. Macroscopic colonies were visualized by staining with 0.005% crystal violet solution and colonies ≥0.5 mm were manually counted.

Tumorigenesis Assay

A total of 1.5 × 10^6 dp53R-shSCR or dp53R-shARF MEFs were resuspended in PBS and injected into the flanks of female homozygous athymic nude mice (*Foxn1*^{nu}/*Foxn1*^{nu}) obtained from Jackson Laboratory. Five mice per condition were used. Tumor size was monitored over the course of 20 days using calipers to measure in two dimensions. Tumor volume was calculated using the formula: volume = [(height)^2 × length]/2, in which height equals the smallest of the two measurements.

Microarray Analysis

RNA was isolated from dp53R-shSCR or dp53R-shARF MEFs using a Nucleospin RNA II Kit (Clonetech). RNA samples from three independent experiments were submitted to the Genome Technology Access Center at Washington University School of Medicine for microarray analysis. Affymetrix Gene 1.0ST arrays were used, and data were processed in Affymetrix Expression Console (Affymetrix version) using the RMA (robust multichip average) algorithm. Differential expression analysis was performed using significant analysis of microarrays, and a list of differentially expressed genes exhibiting fold changes greater than 2 was generated. Pathway analysis was performed using MetaCore software (Thomson Reuters).

Quantitative Real-Time PCR

qRT-PCR was performed as previously described (Miceli et al., 2012). Fold change was measured using the $\Delta\Delta C_T$ method. Primer sequences used for amplification were as follows: *Arf*, forward (Fwd) 5′-GAGTACAGCAGCGGGA GCAT-3′ reverse (Rev) 5′-ATCATCATCACCTGGTCCAGGATTCC-3′; *Trp53*, Fwd 5′-CATCACCTCACTGCATGGAC-3′ Rev 5′-AAAAGATGACAGGGGCC ATG-3′; *β-Actin*, Fwd 5′-TCACCCACACTGTGCCCATCTA-3′ Rev 5′-TAC TCCTGCTTGCTGATCCACA-3′; *Histone 3.3*, Fwd 5′-CGTGAAATCAGACGC TAGCAGAA-3′ Rev 5′-TCGCACCAGACGCTGAAAG-3′; *Oasl2*, Fwd 5′-ATC ATTGTCCTTACCCACAGAG-3′ Rev 5′-TGCTGGTTTTGAGTCTCTGG-3′; *Isg15*, Fwd 5′-CTGACTGTGAGAGCAAGCAGC-3′ Rev 5′-ACCAATCTTCTGG GCAATCTG-3′; *Ifit3*, Fwd 5′-AGCACAGAAACAGATCACCAT-3′ Rev 5′-CAC CCTGTCTTCCATATGACTG-3′; *Usp18*, Fwd 5′-TTCCCTCAGAGCTTGGAT TTC-3′ Rev 5′-CCGGATGTAGGCACAGTAATG-3′; *Irf7*, Fwd 5′-TTGATCCG CATAAGGTGTACG-3′ Rev 5′-TTCCCTATTTTCCGTGGCTG-3′; *Sfrp2*, Fwd 5′-GCCTGCAAAACCAAGAATGAG-3′ Rev 5′-GTCTTGCTCTTTGTCTCCA GG-3′; *Stat1*, Fwd 5′-GCCGAGAACATACCAGAGAATC-3′ Rev 5′-GATGTAT CCAGTTCGCTTAGGG-3′; *Ifnb1*, Fwd 5′-CCACCACAGCCCTCTCCATCAACT AT-3′ Rev 5′-CAAGTGGAGAGCAGTTGAGGACATC-3′; *Il6*, Fwd 5′-CAAAG CCAGAGTCCTTCAGAG-3′ Rev 5′-GTCCTTAGCCACTCCTTCTG-3′; *Tgtp1*,

Fwd 5′-CGAGTACTGGGAAGCTTGAAA-3′ Rev 5′-ATCAGGAGAAGGGAAAGCATG-3′.

IFN-β ELISA

Cell culture supernatants were concentrated using Vivaspin columns (GE Healthcare) according to the manufacturer's instructions. Mouse IFN-β levels were measured using the Verikine Mouse Interferon Beta ELISA Kit (PBL Interferon Source) according to the manufacturer's instructions.

Immunohistochemistry

Annotated breast cancer tissue arrays were obtained from US Biomax (Cat#BR1503a). Staining was performed using the Dako EnVision+ System-HRP (DAB) according to the manufacturer's instructions. Rabbit anti-p14ARF (Bethyl) and mouse anti-iSG15 (Santa Cruz) were used at a 1:200 dilution. Quantification was performed by two separate individuals by blindly scoring staining intensity on a 0–3 scale, with 0 being no staining and 3 being strong widespread staining. A score of 0–1 was considered "low/no" staining, and a score of 2–3 was considered "high."

Statistical Analysis.

Data are presented as means ± SD. Statistical differences between groups were determined with p values obtained using two-sided, unpaired Student's t test. All data points represent n = 3. All images presented as "representative" were completed a minimum of three times.

ACCESSION NUMBERS

The NCBI Gene Expression Omnibus accession number for the microarray data reported in this paper is GSE48315.

SUPPLEMENTAL INFORMATION

Supplemental Information includes Supplemental Experimental Procedures, six figures, and one table and can be found with this article online at http://dx.doi.org/10.1016/j.celrep.2014.03.026.

ACKNOWLEDGMENTS

We thank Scott Werneke and Deborah Lenschow for generously providing the ISG15 antibody. We also thank Michael Kuchenreuther, Alexander Miceli, and other members of the Weber laboratory for technical assistance. We are grateful to Josh Rubin and Greg Longmore for critical suggestions. This work was supported by National Institutes of Health (NIH) grant R01CA120436 and the Department of Defense Era of Hope Scholar grant to J.D.W. L.B.M. was supported by National Cancer Institute grant 1K12CA167540 and a Clinical and Translational Science Award (UL1RR024992) from the NIH. J.T.F. was supported by NIH grant 5T32GM007067.

Received: August 9, 2013
Revised: January 28, 2014
Accepted: March 10, 2014
Published: April 10, 2014

REFERENCES

Apicelli, A.J., Maggi, L.B., Jr., Hirbe, A.C., Miceli, A.P., Olanich, M.E., Schulte-Winkeler, C.L., Saporita, A.J., Kuchenreuther, M., Sanchez, J., Weilbaecher, K., and Weber, J.D. (2008). A non-tumor suppressor role for basal p19ARF in maintaining nucleolar structure and function. Mol. Cell. Biol. *28*, 1068–1080.

Buess, M., Nuyten, D.S., Hastie, T., Nielsen, T., Pesich, R., and Brown, P.O. (2007). Characterization of heterotypic interaction effects in vitro to deconvolute global gene expression profiles in cancer. Genome Biol. *8*, R191.

Burks, J., Reed, R.E., and Desai, S.D. (2014). ISGylation governs the oncogenic function of Ki-Ras in breast cancer. Oncogene *33*, 794–803.

Cancer Genome Atlas Research Network (2012). Comprehensive genomic characterization of squamous cell lung cancers. Nature *489*, 519–525.

Chan, S.R., Vermi, W., Luo, J., Lucini, L., Rickert, C., Fowler, A.M., Lonardi, S., Arthur, C., Young, L.J., Levy, D.E., et al. (2012). STAT1-deficient mice spontaneously develop estrogen receptor α-positive luminal mammary carcinomas. Breast Cancer Res. *14*, R16.

Cheon, H., Holvey-Bates, E.G., Schoggins, J.W., Forster, S., Hertzog, P., Imanaka, N., Rice, C.M., Jackson, M.W., Junk, D.J., and Stark, G.R. (2013). IFNβ-dependent increases in STAT1, STAT2, and IRF9 mediate resistance to viruses and DNA damage. EMBO J. *32*, 2751–2763.

Chiappinelli, K.B., Haynes, B.C., Brent, M.R., and Goodfellow, P.J. (2012). Reduced DICER1 elicits an interferon response in endometrial cancer cells. Mol. Cancer Res. *10*, 316–325.

Duarte, C.W., Willey, C.D., Zhi, D., Cui, X., Harris, J.J., Vaughan, L.K., Mehta, T., McCubrey, R.O., Khodarev, N.N., Weichselbaum, R.R., and Gillespie, G.Y. (2012). Expression signature of IFN/STAT1 signaling genes predicts poor survival outcome in glioblastoma multiforme in a subtype-specific manner. PLoS ONE *7*, e29653.

Dunn, G.P., Koebel, C.M., and Schreiber, R.D. (2006). Interferons, immunity and cancer immunoediting. Nat. Rev. Immunol. *6*, 836–848.

Durbin, J.E., Hackenmiller, R., Simon, M.C., and Levy, D.E. (1996). Targeted disruption of the mouse Stat1 gene results in compromised innate immunity to viral disease. Cell *84*, 443–450.

Ellis, M.J., and Perou, C.M. (2013). The genomic landscape of breast cancer as a therapeutic roadmap. Cancer Discov. *3*, 27–34.

Jonkers, J., Meuwissen, R., van der Gulden, H., Peterse, H., van der Valk, M., and Berns, A. (2001). Synergistic tumor suppressor activity of BRCA2 and p53 in a conditional mouse model for breast cancer. Nat. Genet. *29*, 418–425.

Kamijo, T., Zindy, F., Roussel, M.F., Quelle, D.E., Downing, J.R., Ashmun, R.A., Grosveld, G., and Sherr, C.J. (1997). Tumor suppression at the mouse INK4a locus mediated by the alternative reading frame product p19ARF. Cell *91*, 649–659.

Kawagishi, H., Nakamura, H., Maruyama, M., Mizutani, S., Sugimoto, K., Takagi, M., and Sugimoto, M. (2010). ARF suppresses tumor angiogenesis through translational control of VEGFA mRNA. Cancer Res. *70*, 4749–4758.

Kuchenreuther, M.J., and Weber, J.D. (2014). The ARF tumor-suppressor controls Drosha translation to prevent Ras-driven transformation. Oncogene *33*, 300–307.

Kuo, M.L., den Besten, W., Thomas, M.C., and Sherr, C.J. (2008). Arf-induced turnover of the nucleolar nucleophosmin-associated SUMO-2/3 protease Senp3. Cell Cycle *7*, 3378–3387.

Leonova, K.I., Brodsky, L., Lipchick, B., Pal, M., Novototskaya, L., Chenchik, A.A., Sen, G.C., Komarova, E.A., and Gudkov, A.V. (2013). p53 cooperates with DNA methylation and a suicidal interferon response to maintain epigenetic silencing of repeats and noncoding RNAs. Proc. Natl. Acad. Sci. USA *110*, E89–E98.

Marotta, L.L., Almendro, V., Marusyk, A., Shipitsin, M., Schemme, J., Walker, S.R., Bloushtain-Qimron, N., Kim, J.J., Choudhury, S.A., Maruyama, R., et al. (2011). The JAK2/STAT3 signaling pathway is required for growth of $CD44^{+}CD24^{-}$ stem cell-like breast cancer cells in human tumors. J. Clin. Invest. *121*, 2723–2735.

Miceli, A.P., Saporita, A.J., and Weber, J.D. (2012). Hypergrowth mTORC1 signals translationally activate the ARF tumor suppressor checkpoint. Mol. Cell. Biol. *32*, 348–364.

O'Dell, M.R., Huang, J.L., Whitney-Miller, C.L., Deshpande, V., Rothberg, P., Grose, V., Rossi, R.M., Zhu, A.X., Land, H., Bardeesy, N., and Hezel, A.F. (2012). Kras(G12D) and p53 mutation cause primary intrahepatic cholangiocarcinoma. Cancer Res. *72*, 1557–1567.

Osiak, A., Utermöhlen, O., Niendorf, S., Horak, I., and Knobeloch, K.P. (2005). ISG15, an interferon-stimulated ubiquitin-like protein, is not essential for STAT1 signaling and responses against vesicular stomatitis and lymphocytic choriomeningitis virus. Mol. Cell. Biol. *25*, 6338–6345.

Perou, C.M., Jeffrey, S.S., van de Rijn, M., Rees, C.A., Eisen, M.B., Ross, D.T., Pergamenschikov, A., Williams, C.F., Zhu, S.X., Lee, J.C., et al. (1999). Distinctive gene expression patterns in human mammary epithelial cells and breast cancers. Proc. Natl. Acad. Sci. USA *96*, 9212–9217.

Platanias, L.C. (2005). Mechanisms of type-I- and type-II-interferon-mediated signalling. Nat. Rev. Immunol. *5*, 375–386.

Qi, Y., Gregory, M.A., Li, Z., Brousal, J.P., West, K., and Hann, S.R. (2004). p19ARF directly and differentially controls the functions of c-Myc independently of p53. Nature *431*, 712–717.

Quelle, D.E., Zindy, F., Ashmun, R.A., and Sherr, C.J. (1995). Alternative reading frames of the INK4a tumor suppressor gene encode two unrelated proteins capable of inducing cell cycle arrest. Cell *83*, 993–1000.

Ramana, C.V., Chatterjee-Kishore, M., Nguyen, H., and Stark, G.R. (2000). Complex roles of Stat1 in regulating gene expression. Oncogene *19*, 2619–2627.

Riley, T., Sontag, E., Chen, P., and Levine, A. (2008). Transcriptional control of human p53-regulated genes. Nat. Rev. Mol. Cell Biol. *9*, 402–412.

Roussel, M.F. (1999). The INK4 family of cell cycle inhibitors in cancer. Oncogene *18*, 5311–5317.

Rozenblum, E., Schutte, M., Goggins, M., Hahn, S.A., Panzer, S., Zahurak, M., Goodman, S.N., Sohn, T.A., Hruban, R.H., Yeo, C.J., and Kern, S.E. (1997). Tumor-suppressive pathways in pancreatic carcinoma. Cancer Res. *57*, 1731–1734.

Sadler, A.J., and Williams, B.R. (2008). Interferon-inducible antiviral effectors. Nat. Rev. Immunol. *8*, 559–568.

Sanchez-Cespedes, M., Reed, A.L., Buta, M., Wu, L., Westra, W.H., Herman, J.G., Yang, S.C., Jen, J., and Sidransky, D. (1999). Inactivation of the INK4A/ARF locus frequently coexists with TP53 mutations in non-small cell lung cancer. Oncogene *18*, 5843–5849.

Saporita, A.J., Maggi, L.B., Jr., Apicelli, A.J., and Weber, J.D. (2007). Therapeutic targets in the ARF tumor suppressor pathway. Curr. Med. Chem. *14*, 1815–1827.

Selbert, S., Bentley, D.J., Melton, D.W., Rannie, D., Lourenço, P., Watson, C.J., and Clarke, A.R. (1998). Efficient BLG-Cre mediated gene deletion in the mammary gland. Transgenic Res. *7*, 387–396.

Sherr, C.J. (2001). The INK4a/ARF network in tumour suppression. Nat. Rev. Mol. Cell Biol. *2*, 731–737.

Sherr, C.J. (2006). Divorcing ARF and p53: an unsettled case. Nat. Rev. Cancer *6*, 663–673.

Sherr, C.J., Bertwistle, D., DEN Besten, W., Kuo, M.L., Sugimoto, M., Tago, K., Williams, R.T., Zindy, F., and Roussel, M.F. (2005). p53-dependent and -independent functions of the Arf tumor suppressor. Cold Spring Harb. Symp. Quant. Biol. *70*, 129–137.

Stott, F.J., Bates, S., James, M.C., McConnell, B.B., Starborg, M., Brookes, S., Palmero, I., Ryan, K., Hara, E., Vousden, K.H., and Peters, G. (1998). The alternative product from the human CDKN2A locus, p14(ARF), participates in a regulatory feedback loop with p53 and MDM2. EMBO J. *17*, 5001–5014.

Sugimoto, M., Kuo, M.L., Roussel, M.F., and Sherr, C.J. (2003). Nucleolar Arf tumor suppressor inhibits ribosomal RNA processing. Mol. Cell *11*, 415–424.

Tsai, Y.C., Pestka, S., Wang, L.H., Runnels, L.W., Wan, S., Lyu, Y.L., and Liu, L.F. (2011). Interferon-β signaling contributes to Ras transformation. PLoS ONE *6*, e24291.

Weber, J.D., Jeffers, J.R., Rehg, J.E., Randle, D.H., Lozano, G., Roussel, M.F., Sherr, C.J., and Zambetti, G.P. (2000). p53-independent functions of the p19(ARF) tumor suppressor. Genes Dev. *14*, 2358–2365.

Yu, H., Pardoll, D., and Jove, R. (2009). STATs in cancer inflammation and immunity: a leading role for STAT3. Nat. Rev. Cancer *9*, 798–809.

Zeng, Y., Kotake, Y., Pei, X.H., Smith, M.D., and Xiong, Y. (2011). p53 binds to and is required for the repression of Arf tumor suppressor by HDAC and polycomb. Cancer Res. *71*, 2781–2792.

Zimmerman, M.A., Rahman, N.T., Yang, D., Lahat, G., Lazar, A.J., Pollock, R.E., Lev, D., and Liu, K. (2012). Unphosphorylated STAT1 promotes sarcoma development through repressing expression of Fas and bad and conferring apoptotic resistance. Cancer Res. *72*, 4724–4732.

Zindy, F., Quelle, D.E., Roussel, M.F., and Sherr, C.J. (1997). Expression of the p16INK4a tumor suppressor versus other INK4 family members during mouse development and aging. Oncogene *15*, 203–211.

Zindy, F., Eischen, C.M., Randle, D.H., Kamijo, T., Cleveland, J.L., Sherr, C.J., and Roussel, M.F. (1998). Myc signaling via the ARF tumor suppressor regulates p53-dependent apoptosis and immortalization. Genes Dev. *12*, 2424–2433.

Cell Reports, Volume *7*

Supplemental Information

ARF and p53 Coordinate Tumor Suppression of an Oncogenic IFN-β-STAT1-ISG15 Signaling Axis

Jason T. Forys, Catherine E. Kuzmicki, Anthony J. Saporita, Crystal L. Winkeler, Leonard B. Maggi, Jr., and Jason D. Weber

SUPPLEMENTAL EXPERIMENTAL PROCEDURES

Mice. All animal studies were performed according to the guidelines established by the Animal Studies Committee at Washington University in St. Louis. *Arf* $^{flox/flox}$ mice were generously provided by Dr. Charles Sherr (St. Jude Children's Research Hospital), and have been described previously (Gromley et al., 2009). Mice expressing Cre-recombinase under the control of the beta-lactoglobulin promoter (BLG) were provided by Dr. Christine Watson (University of Cambridge), and have been previously described (Selbert et al., 1998).

***Blg*-Cre mammary tumor model.** Mice were bred to obtain female cohorts of *Blg-Cre;p53*$^{flox/flox}$ *;Arf* $^{+/+}$ and *Blg-Cre;p53*$^{flox/flox}$ *;Arf* $^{flox/flox}$ animals (n=4 per group). These mice were then bred to activate expression of Cre-recombinase specifically in the mammary epithelium. The animals were monitored for mammary tumor formation and sacrificed when tumors reached 2cm. Tumor DNA was extracted using a QIAamp DNA Mini kit (Qiagen). PCR genotyping for floxed alleles and Cre-mediated recombination was performed exactly as described (Jonkers et al., 2001; Winkeler et al., 2012). Tumor RNA was isolated using RNA-Solv (Omega Bio-Tek) according to the manufacturer's instructions.

Lentiviral shRNAs. The sequences of additional shRNAs used in supplemental figures are as follows: shARF-C7 5'-GTCTTTGTGTACCGCTGGGAA-3' shISG15-1 (human) 5'-GCGCAGATCACCCAGAAGATT-3' shISG15-2 (human) 5'-CTGAGCATCCTGGTGAGGAAT-3'. The p16 shRNA was designed using the SciTools RNAi Design tool from Integrated DNA Technologies (IDT), limiting the selection to Exon 1 alpha of p16. The sequence is as follows: 5'-CCG GCT CGA GGA GAG CCA TCT GGA GCA GCA TCT CGA GAT GCT GCT CCA GAT GGC TCT CCT GCA GTT TTT G-3'. The underlined bases represent the targeting 27mer. This and its complement were annealed and cloned into

pKLO.1 at the AgeI and Eco RI sites. Lentivirus production and infection was performed as described in the Experimental Procedures.

SUPPLEMENTAL FIGURE LEGENDS

Figure S1 (Related to Figure 3) ISG induction following ARF depletion is specific to *p53*-deficient setting.
(A) mRNA from dp53 MEFs infected with mock (no virus), empty vector, or Ras^{V12} expressing retrovirus was analyzed by qRT-PCR. Relative mRNA expression levels were obtained by normalizing to Histone 3.3 mRNA. Fold changes are relative to mock-infected control.
(B) mRNA from *Arf*-null MEFs infected with mock, shSCR, or shARF lentivirus was analyzed by qRT-PCR. Relative mRNA expression levels were obtained as described in (A).
(C) Wild-type MEFs were infected with shSCR or shARF and harvested 4 days post-infection. Relative mRNA levels were determined by performing qRT-PCR with extracted RNA. Fold changes are relative to shSCR and normalized to Histone 3.3 mRNA.
(D) mRNA from three independent sets of low passage (<P6) Wild type or *Arf*-null MEFs was analyzed by qRT-PCR for the indicated genes. Relative mRNA expression was obtained as described in (A).
(E) mRNA from dp53 MEFs infected with mock (no virus), shSCR, or shARF lentivirus was analyzed by qRT-PCR. Relative mRNA expression levels were obtained as described in (A). All error bars represent s.d. of n=3.

Figure S2 (Related to Figure 3) P16 does not regulate ISG expression in response to *p53* loss.
(A) Western blot analysis of $p53^{flox/flox}$ MEFs infected with Adeno-LacZ (L) or Adeno-Cre (C) followed by infection with shSCR or shARF as indicated.
(B) Dp53 MEFs expressing empty-vector or Ras^{V12} were infected with shSCR, shARF, or a hairpin targeting both p16 and ARF (shARF-C7). A representative western blot for the indicated proteins is shown.
(C) Quantitative real-time PCR analysis of the cells described in (B). Fold changes of the indicated mRNAs are relative to shSCR controls and normalized to histone 3.3 mRNA levels.
(D) dp53R MEFs were infected with shARF, shp16, or shSCR control and mRNA levels of two ISGs were measured by qRT-PCR. Fold changes were determined by normalizing to histone 3.3 mRNA and are relative to shSCR controls. Error bars represent s.d. from two independent experiments.
(E) Western blot analysis of cells described in (D).

Figure S3 (Related to Figure 3) Combinatorial loss of *p53* and *Arf* in mouse mammary tumors induces ISG15 mRNA.
(A) Mammary tumor or tail DNA isolated from *Blg-Cre;p53$^{flox/flox}$;Arf $^{+/+}$* (n=4) and *Blg-Cre;p53$^{flox/flox}$;Arf $^{flox/flox}$* (n=4) mice was subjected to PCR analysis for genotyping. Cre-mediated recombination of p53 (*p53$^{\Delta 2\text{-}10}$*) and Arf (*Arf $^{\Delta Exon\ 1\text{-}\beta}$*) was assessed by PCR to validate the genotypes of the tumor-bearing cohorts.
(B) RNA extracted from tumors was analyzed by qRT-PCR. Fold change of ISG15 is presented relative to *Blg-Cre;p53$^{flox/flox}$;Arf $^{+/+}$* tumors and values were normalized to histone 3.3. mRNA levels. Error bars respresent s.d. of n=4.

Figure S4 (Related to Figure 5). Neither STAT3 activation nor IL-6 expression are enhanced in dp53R-shARF MEFs.
(A) Western blot analysis of dp53R-shSCR or shARF MEFs for evidence of STAT3 activation.
(B) qRT-PCR analysis of cells from (A) for expression of the cytokine, IL-6 normalized to Histone 3.3. Error bars represent s.d. of three independent measurements.

Figure S5 (Related to Figure 7) Analysis of TNBC cell lines.
(A) Western blot analysis of a panel of triple negative breast cancer cell lines blotted with indicated antibodies. Human mammary epithelial cells (HMECs) were used as a normal control.
(B) Light microscopy images of HCC1806 cells infected with STAT1 hairpins displaying morphological evidence of apoptosis/necrosis.
(C) Western blot in MB-231 cells depleted of STAT1 showing STAT3 levels are unaffected by the shRNAs.

Figure S6 (Related to Figure 7) HCC70 cells are sensitive to ISG15 depletion.
(A) Western blot analysis of HCC70 cells expressing two independent STAT1 shRNAs.
(B) Western blot analysis of HCC70 cells expressing two independent ISG15 shRNAs.
(C) HCC70 cells were infected with two ISG15 shRNAs or a scrambled control and plated for a proliferation assay. Cells were trypsinized and counted on the indicated number of days post plating. Error bars represent s.d. of n=3.

Table S1 (Related to Figure 7). Raw IHC data from TNBC tumor samples

SUPPLEMENTAL TABLES

SUPPLEMENTAL FIGURES

Gromley, A., Churchman, M.L., Zindy, F., and Sherr, C.J. (2009). Transient expression of the Arf tumor suppressor during male germ cell and eye development in Arf-Cre reporter mice. Proceedings of the National Academy of Sciences of the United States of America *106*, 6285-6290.

Jonkers, J., Meuwissen, R., van der Gulden, H., Peterse, H., van der Valk, M., and Berns, A. (2001). Synergistic tumor suppressor activity of BRCA2 and p53 in a conditional mouse model for breast cancer. Nature genetics *29*, 418-425.

Selbert, S., Bentley, D.J., Melton, D.W., Rannie, D., Lourenco, P., Watson, C.J., and Clarke, A.R. (1998). Efficient BLG-Cre mediated gene deletion in the mammary gland. Transgenic research *7*, 387-396.

Winkeler, C.L., Kladney, R.D., Maggi, L.B., Jr., and Weber, J.D. (2012). Cathepsin K-Cre causes unexpected germline deletion of genes in mice. PloS one *7*, e42005.

Figure S1. Forys et al.

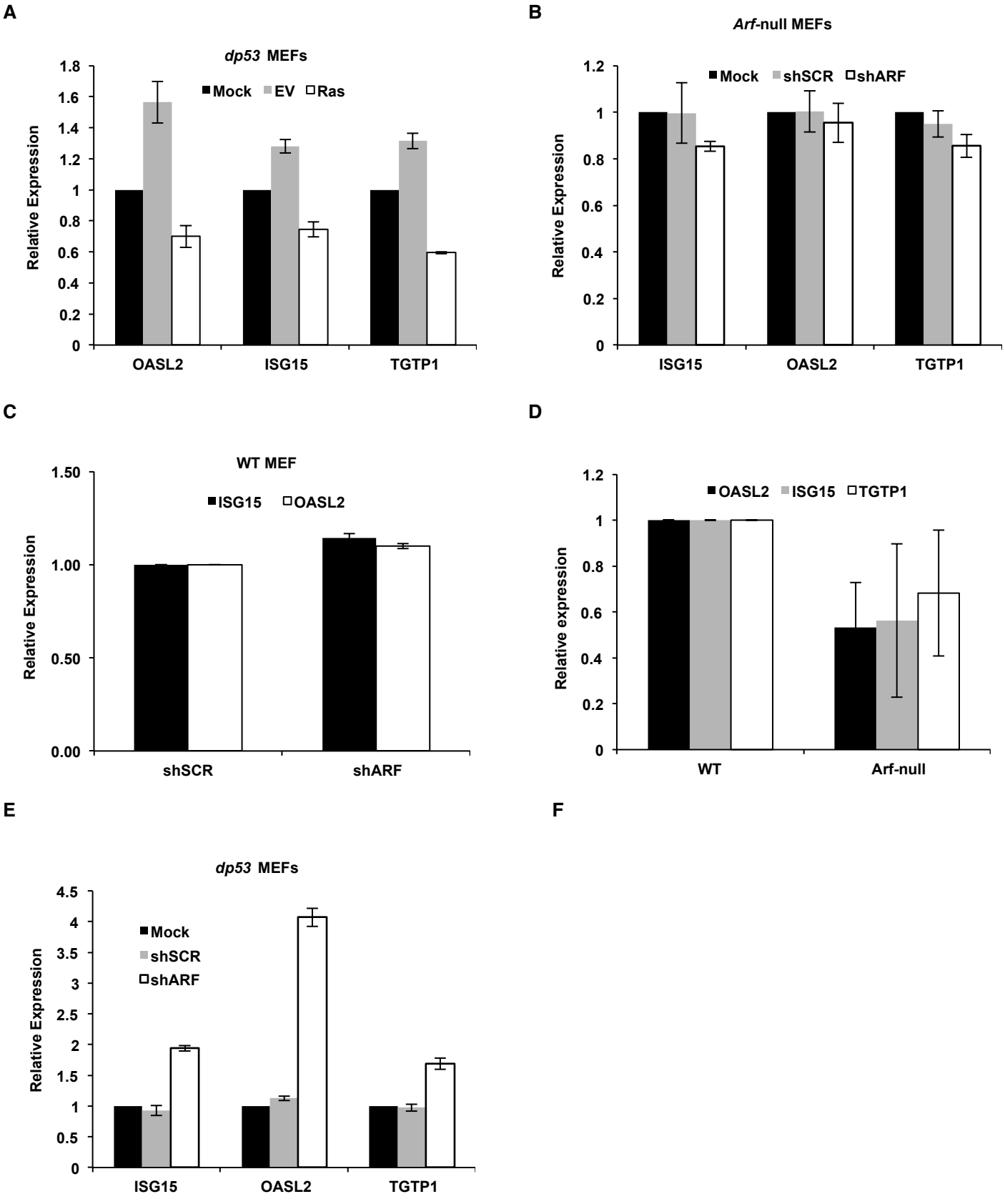

Figure S2. Forys et al.

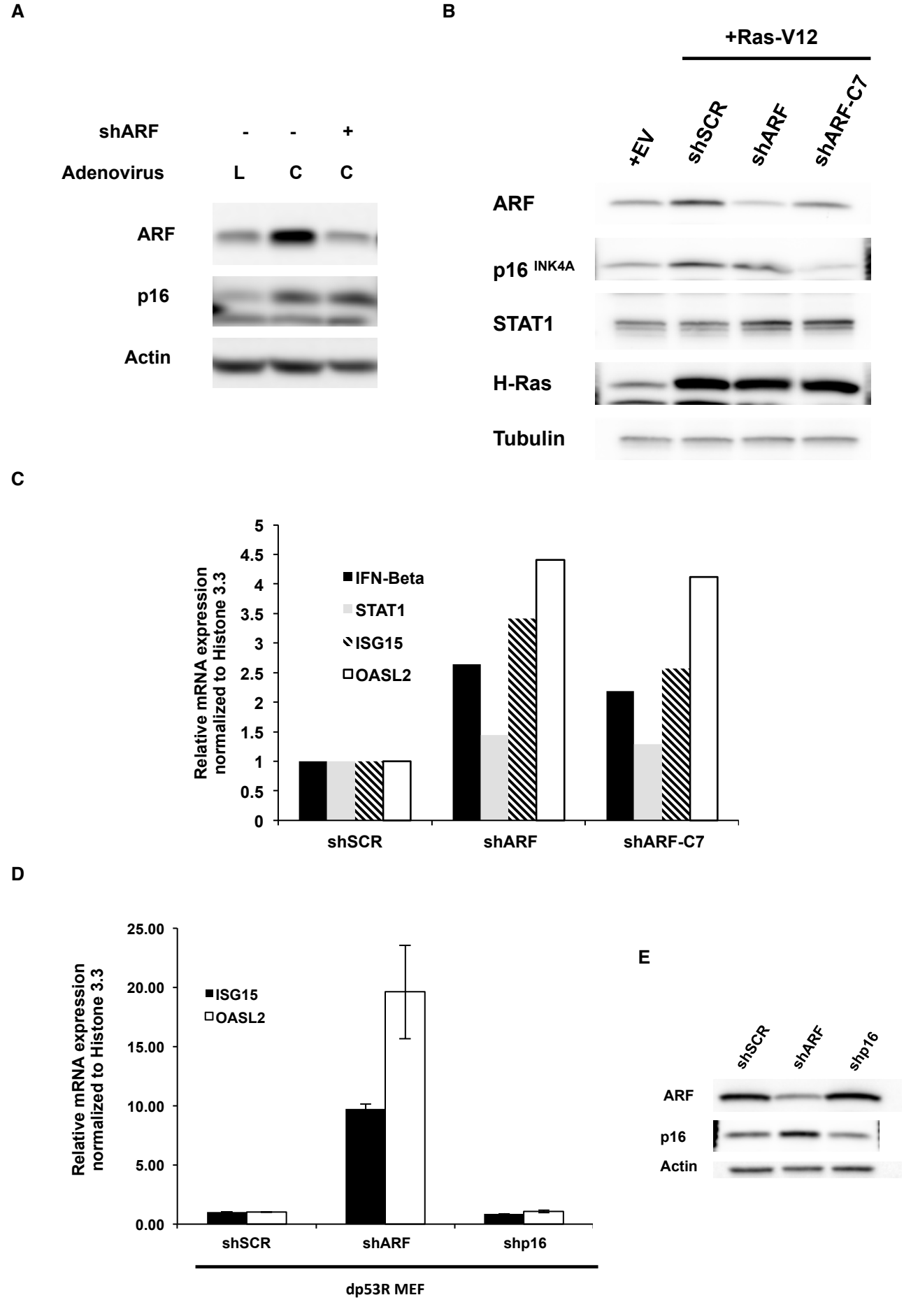

Figure S3. Forys et al.

A

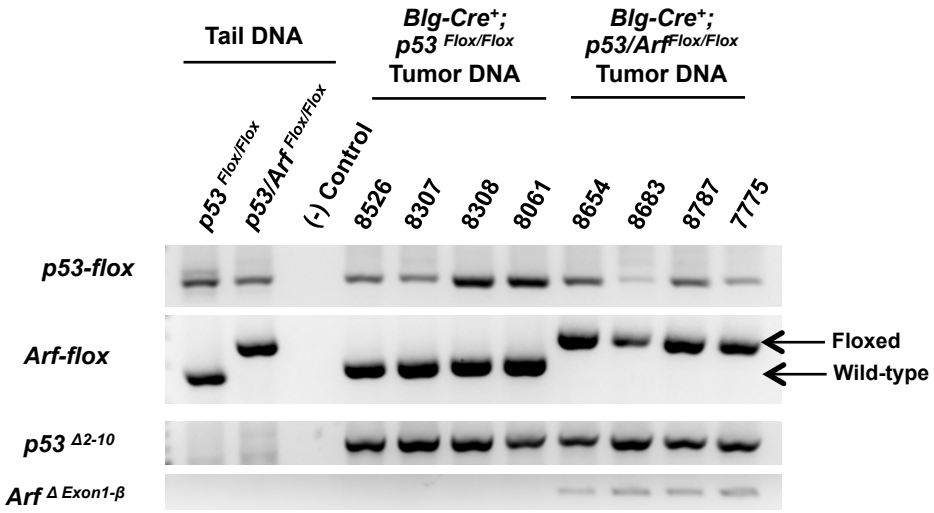

B

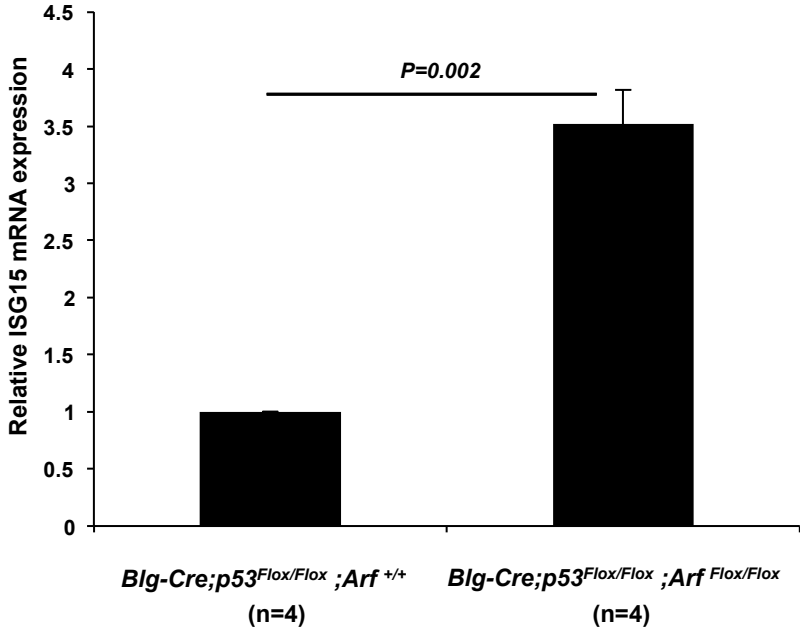

Figure S4. Forys et al.

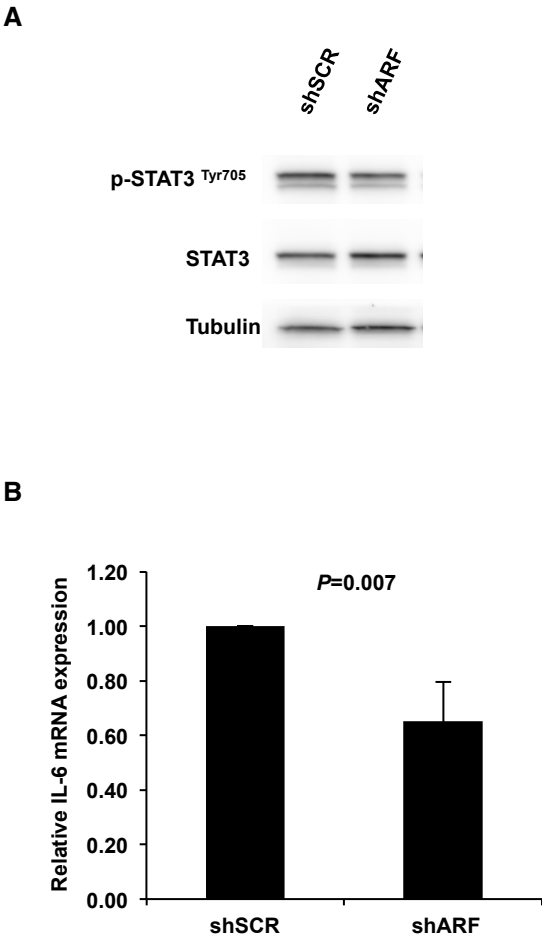

Figure S5. Forys et al.

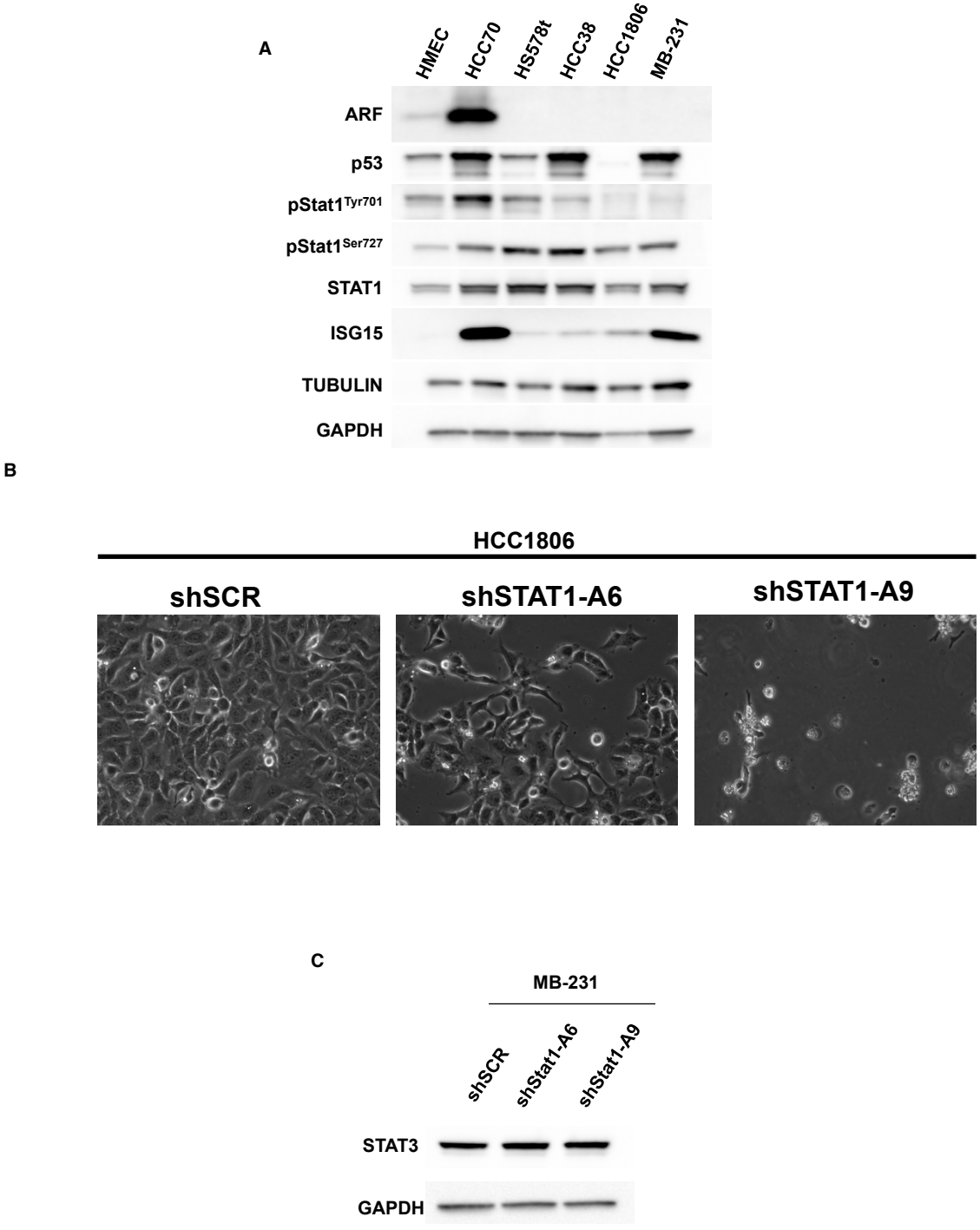

Figure S6. Forys et al.

A

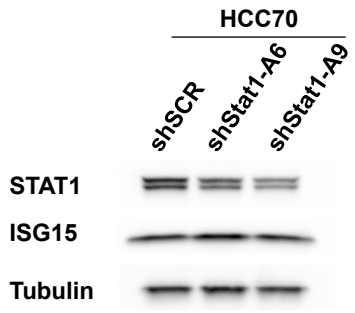

B

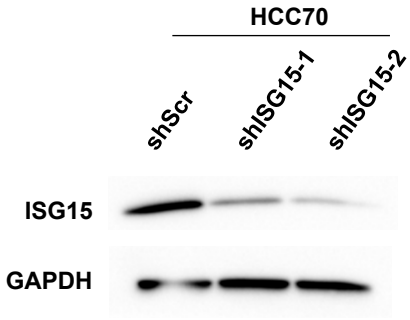

C

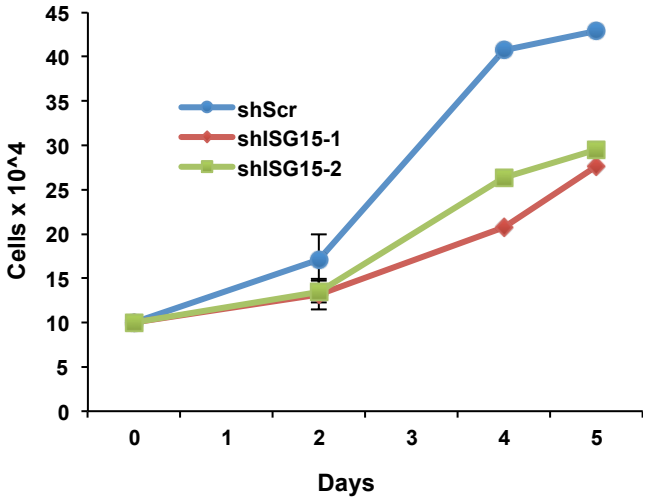

Table S1. Forys et al.

TUMOR #	p53	ARF	STAT1	ISG15
1	+++, 90%	1	3	2
2	+++, 100%	0	3	2
3	++, 75%	1	2	1
4	+, 90%	1	1	1
5	+, 90%	1	1	1
6	+, 50%	2	1	1
7	+++, 70%	0	2	2
8	+++, 60%	1	1	1
9	+, 15%	2	1	2
10	++, 40%	0	2	3
11	++, 15%	0	1	2
12	++, 15%	1	1	0
13	++, 1.5%	1	1	1